Quaternary Geochronology 30 (2015) 100–113

Contents lists available at ScienceDirect

Quaternary Geochronology

journal homepage: www.elsevier.com/locate/quageo

Research paper

A multi-nuclide approach to constrain landscape evolution and past erosion rates in previously glaciated terrains

Mads Faurschou Knudsen [a, *], David L. Egholm [a], Bo Holm Jacobsen [a], Nicolaj Krog Larsen [a], John D. Jansen [b], Jane Lund Andersen [a], Henriette C. Linge [c]

[a] Department of Geoscience, Aarhus University, Denmark
[b] Institute of Earth and Environmental Science, University of Potsdam, Germany
[c] Department of Earth Science, University of Bergen, Norway

ARTICLE INFO

Article history:
Received 24 February 2015
Received in revised form
14 August 2015
Accepted 30 August 2015
Available online 2 September 2015

Keywords:
Cosmogenic-nuclide geochronology
Markov Chain Monte Carlo inversion
Glacial landscape history
Erosion rate reconstructions
Quaternary climate

ABSTRACT

Cosmogenic nuclides are typically used to either constrain an exposure age, a burial age, or an erosion rate. Constraining the landscape history and past erosion rates in previously glaciated terrains is, however, notoriously difficult because it involves a large number of unknowns. The potential use of cosmogenic nuclides in landscapes with a complex history of exposure and erosion is therefore often quite limited. Here, we present a novel multi-nuclide approach to study the landscape evolution and past erosion rates in terrains with a complex exposure history, particularly focusing on regions that were repeatedly covered by glaciers or ice sheets during the Quaternary. The approach, based on the Markov Chain Monte Carlo (MCMC) technique, focuses on mapping the range of landscape histories that are consistent with a given set of measured cosmogenic nuclide concentrations. A fundamental assumption of the model approach is that the exposure history at the site/location can be divided into two distinct regimes: i) interglacial periods characterized by zero shielding due to overlying ice and a uniform interglacial erosion rate, and ii) glacial periods characterized by 100% shielding and a uniform glacial erosion rate. We incorporate the exposure history in the model framework by applying a threshold value to the global marine benthic $\delta^{18}O$ record and include the threshold value as a free model parameter, hereby taking into account global changes in climate. However, any available information on the glacial-interglacial history at the sampling location, in particular the timing of the last deglaciation event, is readily incorporated in the model to constrain the inverse problem. Based on the MCMC technique, the model delineates the most likely exposure history, including the glacial and interglacial erosion rates, which, in turn, makes it possible to reconstruct an exhumation history at the site. We apply the model to two landscape scenarios based on synthetic data and two landscape scenarios based on paired $^{10}Be/^{26}Al$ data from West Greenland, which makes it possible to quantify the denudation rate at these locations. The model framework, which currently incorporates any combination of the following nuclides ^{10}Be, ^{26}Al, ^{14}C, and ^{21}Ne, is highly flexible and can be adapted to many different landscape settings. The model framework may also be used in combination with physics-based landscape evolution models to predict nuclide concentrations at different locations in the landscape. This may help validate the landscape models via comparison to measured nuclide concentrations or to devise new effective sampling strategies.

1. Introduction

As global climate cooled during the late Neogene, the surface processes eroding mountain ranges seem to have accelerated substantially (Zhang et al., 2001; Herman et al., 2013). The dramatic fluctuations between glacial and interglacial periods characteristic of the Quaternary altered the erosional dynamics in most of Earth's mountain ranges, in part due to changes in river discharge, shifting vegetation regimes, and the advent of cold-climate processes, including frost weathering and the development of extensive ice masses (Shuster et al., 2005; Thomson et al., 2010). These processes played an important role in shaping many of the remarkable, first-order topographic features observed today, such as the spectacular

* Corresponding author.
E-mail address: mfk@geo.au.dk (M.F. Knudsen).

http://dx.doi.org/10.1016/j.quageo.2015.08.004

fjord and valley landscapes of e.g. Norway, Greenland, and New Zealand.

Efforts to understand the evolution of mountain ranges and their complex links to climate are often hampered by difficulties in quantifying past denudation rates, a parameter that may vary over several orders of magnitude depending on the geological setting and processes that govern the removal of mass (e.g. von Blanckenburg, 2005). In non-glaciated terrains, steady-state denudation rates are typically estimated by use of "in-situ" produced cosmogenic nuclides in samples from bedrock (e.g. Lal, 1991) or alluvial sediments (e.g. von Blanckenburg, 2005). This approach is unviable in terrains periodically covered by large ice masses during glacial periods, because the surface rocks were shielded for unknown lengths of time. In such settings, the concentration of cosmogenic nuclides in bedrock and boulders is generally used to infer an exposure age, typically a deglaciation age, assuming substantial glacial erosion prior to the deglaciation and that the denudation rate since the time of exposure is negligible or that it can be inferred from independent evidence.

Inherited nuclides often represent a problem when estimating exposure ages in landscapes that were repeatedly covered by ice in the past. The problem arises in landscapes characterized by low denudation rates, where a significant amount of the cosmogenic nuclides produced during previous periods of exposure remains in the surface bedrock. This problem may be overcome by collecting paired samples in the field, i.e. sampling both boulders and bedrock, in which case it is often possible to estimate the deglacial age and the amount of inheritance in the bedrock sample. An extension of this approach involves the use of paired cosmogenic nuclides, primarily ^{10}Be and ^{26}Al, which allows estimates of the minimum-limiting exposure duration and minimum-limiting burial duration (e.g. Bierman et al., 1999; Corbett et al., 2013). In this case, the different half-lives and production rates of the nuclides can be used to constrain a total landscape history. Concentrations of ^{10}Be and ^{26}Al have additionally been used to study glacial-interglacial variations in denudation rate in non-glaciated terrains (Hidy et al., 2014).

Several studies have employed paired nuclides to date buried sediments (e.g. Granger and Smith, 2000; Granger, 2006; Haeuselmann et al., 2007) and depositional landscape surfaces (Anderson et al., 1996). Most of these studies rely on ^{10}Be and ^{26}Al, but burial dating schemes involving ^{26}Al–^{10}Be–^{21}Ne also exist (Balco and Shuster, 2009). Braucher et al. (2009) used an in-situ produced ^{10}Be depth profile to determine both an exposure time and a denudation rate, and a versatile Monte Carlo simulator for modeling depth profiles of ^{10}Be or ^{26}Al in sediments is available online (Hidy et al., 2010). None of these approaches, however, focus on resolving landscape history and past denudation rates from bedrock samples collected in terrains that were repeatedly covered by glacial ice in the past.

In this study, we aim to develop a robust and flexible multi-nuclide approach to study landscape evolution in areas characterized by a complex exposure history. The main focus is to constrain the most likely glacial-interglacial landscape history of an area and estimate average glacial and interglacial erosion rates by exploiting the different half-lives and production rates of the various cosmogenic nuclides. For this purpose, a Markov Chain Monte Carlo (MCMC) approach is developed in order to systematically delineate the most likely landscape evolution within the framework of the model.

2. Approach and methods

2.1. Model concept and framework

The basic idea underlying this model framework is to systematically simulate the production and loss of in-situ terrestrial cosmogenic nuclides (TCNs) associated with the glacial-interglacial cycles of the Quaternary and to map the glacial-interglacial landscape histories that are consistent with a given set of measured TCN concentrations. We use the MCMC technique to simulate TCN concentrations associated with a large number of different glacial-interglacial landscape histories, including highly varying glacial and interglacial erosion rates. Based on comparisons to measured concentrations, it is possible to determine the most likely landscape history and associated uncertainties. A key aspect of this approach is to select the right set of model parameters and maintain an optimal balance between the number of observations and model parameters in order to be able to constrain the problem. As too many model parameters will render the problem intractable, some simplifications are required to formulate a balanced and viable computational framework for the forward model, i.e. the computation of TCN concentrations over multiple glacial-interglacial cycles.

In general, the production of TCNs occurs during times of exposure when there is no glacial ice to shield the surface bedrock, whereas the loss of TCNs is due to radioactive decay and erosion (Lal, 1991). A key principle introduced in this study is what we refer to as "two-stage uniformitarianism", meaning that the processes that operated during the Holocene also operated during earlier interglacials with comparable intensity. This simplifying assumption implies that the denudation processes that dominated during the Holocene also dominated during earlier interglacials, and similarly that the denudation processes that dominated during the last glacial period, the so-called Weichsel/Wisconsin glacial period, also dominated during earlier glacial periods. The model concept consequently operates with two erosion rates, an interglacial erosion rate, ε_{int}, and a glacial erosion rate, ε_{gla}. The model concept also assumes that interglacial periods were characterized by 100% exposure and zero shielding due to overlying glaciers, whereas glacial periods were characterized by 100% shielding and no exposure, which would require >10 m of ice for production due to spallation (>50 m for muons). However, the timing of glacial-interglacial transitions at any specific location is often poorly constrained in time, or completely unknown, and these transition times must therefore be incorporated in the model framework as free parameters that vary among the simulations. This can be achieved in several different ways, e.g. by using a purely periodic model with cyclic changes between glacials-interglacials, or by integrating any prior knowledge regarding past transitions between glacials and interglacials. In this study, we propose a general approach to constrain the unknowns related to the timing of past glacial-interglacial transitions based on large-scale changes in the global climate regime.

2.1.1. A two-stage glacial-interglacial model based on global climate

Although past transitions between glacial and interglacial periods at specific locations are often unconstrained, reliable information on large-scale climatic changes during the Quaternary is available from marine δ^{18}O records, indicating when glaciations were widespread and likely to occur. Marine benthic oxygen isotope records have been used in previous studies of the link between geomorphology and climate (e.g. Hancock and Anderson, 2002; Tucker et al., 2011) and to infer the most likely glacial-interglacial history by identifying a transition threshold based on the timing of the last deglaciation (e.g. Kleman and Stroeven, 1997; Fabel et al., 2002). Fabel et al. (2002) use a value of 3.7‰, but such a Pleistocene-Holocene threshold value may not have applied to past glacial-interglacial transitions. In this study, we therefore estimate the most likely glacial-interglacial transitions by incorporating the $\delta^{18}O_{threshold}$ value as a free parameter that is applied iteratively to the stacked marine benthic δ^{18}O record of Lisiecki and Raymo

(2005). The four model parameters in this approach include the following:

$$\mathbf{m} = \left[\varepsilon_{int}, \varepsilon_{gla}, t_{degla}, \delta^{18}O_{threshold}\right]$$

where the $\delta^{18}O_{threshold}$ defines the timing of glacial and interglacial periods via the $\delta^{18}O(t)$ time history, and ε_{int} along with ε_{gla} represent the erosion rates during all non-glaciated and all glaciated periods, respectively. (Fig. 1). Note that the degree of smoothing applied to the $\delta^{18}O$ record influences the number of transitions and the duration of individual glacial-interglacial periods, and it is therefore possible to specify the degree of smoothing applied to the $\delta^{18}O$ record. In principle, the timing of the last deglaciation, defined by model parameter t_{degla}, is redundant because it is defined by the $\delta^{18}O_{threshold}$ value. However, it makes sense to decouple the timing of the last deglaciation from the $\delta^{18}O_{threshold}$, because t_{degla} is often known with reasonable precision and accuracy through ^{10}Be dating of allochthonous boulders (glacial erratics) or studies of terminal moraines (e.g. Corbett et al., 2013; Levy et al., 2014).

2.2. Cosmogenic nuclides in the model framework

The model framework can accommodate any number of TCNs, but is currently based on the following four: ^{10}Be, ^{26}Al, ^{14}C, and ^{21}Ne. In some respect, this combination of nuclides is advantageous because of their different half-lives and production rates (Gosse and Phillips, 2001), which enable their concentrations to integrate different aspects of the glacial-interglacial history. All four nuclides are produced at reasonably well-constrained rates in quartz, which is a very common mineral that is highly resistant to weathering and loss of nuclides after production. Quartz is usually the preferred target mineral for all four nuclides. Beryllium-10 and ^{26}Al are routinely measured with high precision using Accelerator Mass Spectrometry (AMS), whereas ^{21}Ne, which is stable, is measured with high precision using a noble gas mass spectrometer. The main challenge with ^{21}Ne is that significant amounts of a non-cosmogenic component may be present in the samples. This interfering component is usually identified and corrected for using a neon three-isotope diagram (Niedermann et al., 1994, 2002) or via deeply shielded samples that contain no cosmogenic ^{21}Ne, such as from road cuts. The inclusion of in-situ produced ^{14}C is important due to its short half-life of 5730 years, which make this nuclide an especially sensitive Holocene chronometer. It remains challenging to measure in-situ produced ^{14}C, but it is currently achieved at several AMS laboratories around the world.

2.2.1. Cosmogenic nuclide production rates

The cosmogenic nuclides are produced when the surface rock is exposed to a shower of secondary cosmic-ray particles, including neutrons and muons (Lal and Peters, 1967). Upon reaching Earth's surface, these particles interact with atoms in the minerals to produce cosmogenic nuclides. In this study, we include the three most important production mechanisms for the four cosmogenic nuclides mentioned above: nucleonic spallation (spal), negative muon capture (nmc), and fast muons (fm). The production of cosmogenic nuclides decays near-exponentially with depth for all three mechanisms, although at different rates because neutrons have considerably shorter attenuation lengths (Λ) than muons, which penetrate much deeper into the ground (Gosse and Phillips, 2001; Braucher et al., 2011, 2013). Although the theoretical production of TCNs due to muons does not behave as a simple exponential function with depth (Heisinger et al., 2002a, 2002b), it has been shown that reasonable approximations to the theoretical production can be made with multiple exponential terms for muon production mechanisms (Granger and Smith, 2000; Schaller et al., 2002). In this study, we follow the general approach of Hidy et al. (2010) to calculate the TCN production as a function of depth (z), albeit with some minor modifications. We use one exponential term to calculate the spallogenic production rate and three terms for each of the muonic components:

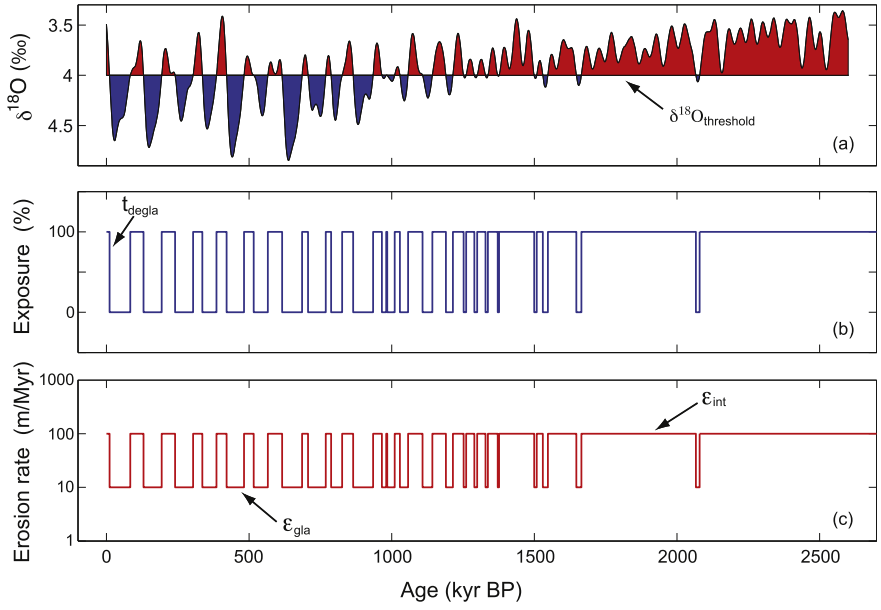

Fig. 1. An example of the two-stage glacial-interglacial model based on the global benthic marine $\delta^{18}O$ record (a). In this approach, the timing and duration (b) of glacial and interglacial periods are defined by a threshold value ($\delta^{18}O_{threshold}$) that is applied to the global marine $\delta^{18}O$ record (Lisiecki and Raymo, 2005). The $\delta^{18}O$ record may be subjected to various degrees of smoothing depending on the landscape setting and prior information. The scenario presented here is based on a 30-kyr running mean of the $\delta^{18}O$ record and a threshold value of 4.0‰. The $\delta^{18}O_{threshold}$ level (a) is a model parameter that is determined as part of the MCMC inversion analysis along with the glacial (ε_{gla}) and interglacial (ε_{int}) erosion rates (c). The timing of the last deglacial event (t_{degla}), which is also a model parameter, is decoupled from the $\delta^{18}O_{threshold}$ level, because t_{degla} is often known with reasonable precision and accuracy from ^{10}Be dating of glacial erratics or other independent evidence.

$$P_{spal}(z) = P_{spal}(0) \times e^{-\frac{\rho z}{\Lambda_{spal}}} \quad (1)$$

$$P_{nmc}(z) = P_{nmc}(0) \times \sum_{i=1}^{3} a_i \times e^{-\frac{\rho z}{\Lambda_{nmc,i}}} \quad (2)$$

$$P_{fm}(z) = P_{fm}(0) \times \sum_{j=1}^{3} b_j \times e^{-\frac{\rho z}{\Lambda_{fm,j}}} \quad (3)$$

$$P_{Total}(z) = P_{spal}(z) + P_{nmc}(z) + P_{fm}(z) \quad (4)$$

where ρ is the density of the rock (here we use a value of 2.65 g/cm^3), Λ the attenuation lengths ($\Lambda_{\sigma\pi\alpha\lambda} = 160$ g/cm^{-2}), and a_i, b_j, are dimensionless coefficients. The values used in this study for the dimensionless coefficients and attenuation lengths associated with negative muon capture (nmc) and fast muons (fm) are adopted from Schaller et al. (2002). We assume that variations in nuclide production rate with depth can be approximated with Eqs. (1)–(4) for all four nuclides. The surface production rates $P(0)_{spal}$, $P(0)_{nmc}$, $P(0)_{fm}$ must be specified for the study site, for instance by use of the CRONUS-Earth on-line calculator (Balco et al., 2008). We note, however, that the current version of our model only incorporates nuclide production rates that are constant in time. This means that scaling schemes accounting for solar and geomagnetic field effects (e.g. Dunai, 2001; Lifton et al., 2005) are excluded for now. The effect of neglecting variations in the solar and geomagnetic fields, however, is small for mid-high latitudes (typically <3%) compared to variations in the TCN production rate among the various production rate models. The effect becomes more pronounced for low-latitude samples that have been subjected to long periods of exposure.

2.2.2. Computation of present TCN concentrations

When erosion rates and TCN production rates at the surface vary as a step function in time due to the waxing and waning of ice sheets, the present-time nuclide concentration may be calculated using a Lagrangian approach in which a layer is tracked as it is slowly advected towards the surface. Consider a rock sample at the present depth of burial, z_{obs}, which for samples collected at the surface will be zero ($z = 0$ m). Owing to the varying erosion rates, $\varepsilon(t)$, this rock sample has followed a depth track given by

$$z(t) = z_{obs} + \int_0^t \varepsilon(t')dt' \quad (5)$$

Therefore, this sample has experienced a production rate that has varied in time according to

$$P(t, z(t)) = P_{spal}(t,0) \times e^{-\rho z(t)/\Lambda_{spal}} + P_{nmc}(t,0) \times e^{-\rho z(t)/\Lambda_{nmc}} + P_{fm}(t,0) \times e^{-\rho z(t)/\Lambda_{fm}} \quad (6)$$

where the production rate at the surface, $P(t,0)$, varies due to changes in the shielding associated with an overlying ice cover, i.e. 0% shielding during interglacials and 100% shielding during glacials. In general, the differential equation for the nuclide concentration is

$$\frac{\partial C(t)}{\partial t} = -\lambda C(t) + P(t, z(t)) \quad (7)$$

where λ is the radioactive decay constant of the nuclide. For a given erosion history and glacial-interglacial exposure history, which govern variations in the surface production rates, it is possible to solve Eq. (7) numerically with standard techniques (see below). However, when the erosion rates and surface production rates are piece-wise constant, this differential equation (Eq. (7)) can be solved analytically by a sum of recursive exponential terms, which makes the calculation of present nuclide concentrations particularly fast for the two-stage glacial-interglacial models considered here.

2.2.3. Numerical validation of the Lagrangian approach to compute TCN concentrations

The present TCN concentrations may also be determined using a Eulerian approach, in which the nuclide concentrations are computed at specific depths while the rock layers are advected towards the surface due to erosion. In this approach, changes in nuclide concentrations are computed in small incremental time steps (dt) as follows

$$\frac{\partial C(t)}{\partial t} = P_{Total}(z) \times dt \times e^{(-\lambda \times dt)} - C(t) \times \lambda \times dt + \varepsilon \times \nabla C(t) \quad (8)$$

where the production term (P_{Total}) includes those nuclides produced within the time step dt, some of which are lost due to decay, and the second term calculates the loss due to decay of existing nuclides. Changes in concentration due to erosion are handled as an upward advection of layers (with $\varepsilon > 0$) with lower concentrations towards the surface, as described by the last term of Eq. (8). This Eulerian approach is a very different, and computationally expensive, way of calculating changes in nuclide concentrations over glacial-interglacial cycles, as the time steps must be relatively small (typically 100 years) to maintain computational stability when computing the advection. The Eulerian approach may, however, serve as a direct way of validating the computation of TCN concentrations based on the Lagrangian approach. Despite their difference, the two methods yield virtually identical TCN concentrations. Fig. 2a demonstrates how the Lagrangian (analytical) approach (red (in web version)) and the step-wise Eulerian approach (blue (in web version)) reach the same ^{10}Be surface concentrations after simulation of 10 glacial-interglacial cycles, lasting 100 kyr and 10 kyr, respectively. Fig. 2b demonstrates how the two approaches yield similar concentrations as a function of depth after simulation of 10 fully periodic glacial-interglacial cycles. As the computational cost represents a critical aspect due to the number of iterations required by the inverse MCMC analysis, we use the analytical solution in the forward computation of TCN concentrations.

3. Markov Chain Monte Carlo inversion analyses

Based on the forward model described above, we have developed an inverse MCMC approach to constrain the most likely landscape history from a combination of cosmogenic nuclides with different production rates and half-lives. The forward models allow for observations of a number of nuclide concentrations and associated uncertainties at a range of depths. The observation data vector consists of the measured nuclide concentrations, which for surface-based measurements ($z = 0$ m) of four nuclides is given by

$$\mathbf{d}_{obs} = [C_{10Be}, C_{26Al}, C_{14C}, C_{21Ne}]$$

We analyze this problem using a conventional Metropolis–Hastings MCMC technique (Metropolis et al., 1953; Hastings, 1970) where model parameters are constrained between fixed

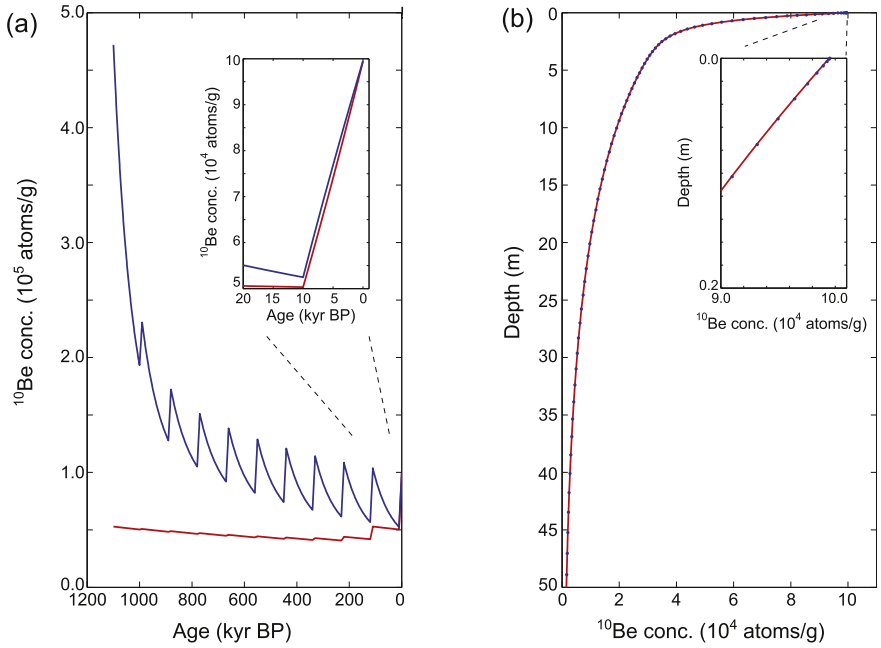

Fig. 2. The forward model is validated numerically by comparing nuclide concentrations calculated by use of two different forward models: the analytical, Lagrangian approach (red), and a numerical, Eulerian approach (blue). The initial concentrations used in these simulations were the depth-dependent ^{10}Be equilibrium concentrations obtained for an erosion rate of 10 m/Myr. Panel A illustrates the Lagragian (red) and Eulerian (blue) approaches to calculate the surface nuclide concentrations for a idealized glacial-interglacial landscape scenario consisting of 10 periodic glacial (100 kyr) and interglacial (10 kyr) cycles. While the Lagrangian approach tracks a certain layer as it moves towards the surface due to erosion, the Eulerian approach calculates the change in concentration with time at certain depths ($z = 0$ m in panel a). As shown in panel b, the two methods yield identical, present-time nuclide concentrations at all depths. (For interpretation of the references to colour in this figure legend, the reader is referred to the web version of this article.)

bounds specified by the user. Erosion rates (ε_{int}, ε_{gla}), which may vary over orders of magnitude, are specified with uniform probability across the logarithmic parameter interval. The time parameters are specified with uniform probability across the linear parameter interval. After the user has specified the bounds of the model parameters, which define the model space that is searched with the MCMC technique, a forward response is computed based on an initial set of model parameters that is proposed using the Metropolis–Hastings technique. A burn-in phase of 1000 iterations is first used to make a crude initial search of the model space. This step is followed by a more detailed and local search of the model space using the set of model parameters from the burn-in phase with the smallest weighted least-squares misfit when compared to the observation data vector. At each iteration step, the current model is perturbed by a fraction of the prior interval. This fraction is updated every 1000 iterations so that an acceptance ratio of about 0.4 is maintained (Gelman et al., 1996). To ensure that the set of model parameters providing the best, weighted least-squares fit to the observed data does not depend on the starting position of the random search through the model space, a number of "random walks" (e.g. 4) are started at different positions in the model space (e.g. different corners or edges). If these completely independent "random walks" achieve similar distributions for the best-fitting model parameters, it is highly unlikely that other global misfit minima remain undetected. Based on the combination of model parameters that provide the best fit to the data, it is possible to compute the most likely exhumation history for the site and/or study area.

4. Investigating synthetic landscape scenarios

Many mountain ranges developed large ice masses as the global climate cooled during the late Neogene. This marked a transition from essentially ice-free conditions to a time of repeated growth and decay of glacial ice over tens of glacial cycles. Depending on latitude, elevation, and regional climate regime, these glaciers may have been warm-based and highly erosive, or cold-based and non-erosive (e.g. Fabel et al., 2002; Kleman et al., 2008). In this section, we illustrate the model approach and associated MCMC technique by simulating synthetic landscape-evolution scenarios that resemble the onset of widespread glaciations, both erosive and non-erosive, during the Quaternary. For the two scenarios studied here, we generate the "observed" nuclide concentrations (^{10}Be, ^{26}Al, ^{14}C, and ^{21}Ne), which form the basis of the MCMC inversion, based on predefined synthetic model parameters. Studies of synthetic data represent an important aspect because they make it possible to test the capability of the inversion procedure. In the synthetic scenarios below, we use the northeastern North

Fig. 3. MCMC inversion results for synthetic landscape scenario 1. The histograms show the distribution of (a) interglacial erosion rates, (b) glacial erosion rate, (c) timing of last deglaciation, and (d) $\delta^{18}O_{threshold}$ levels that provide the best fit to the TCN concentrations in synthetic landscape scenario 1. The fraction indicates the number of simulations included in each bin out of the 10,000 simulations that followed the burn-in phase. (e) The exposure/burial history obtained with the median $\delta^{18}O_{threshold}$ value (d) of the 10,000 simulations in the MCMC inversion analysis. (f) Exhumation histories associated with the best-fitting set of model parameters in the 10,000 simulations (a–d). The depth and time units in (f) were binned and the shading reflects the number of simulations passing through the bins. The black lines in (a–f) denote the median value, whereas the red lines denote the 25% and 75% quartiles. (g) Cumulative contributions during the Quaternary to the present TCN concentrations for synthetic landscape scenario 1 based on the true model parameters (magenta lines in a–d) and true exhumation history (magenta line in f). Note that the short half-life of ^{14}C implies that only the nuclides produced during the Holocene interglacial period contributes to the present ^{14}C concentration. (For interpretation of the references to colour in this figure legend, the reader is referred to the web version of this article.)

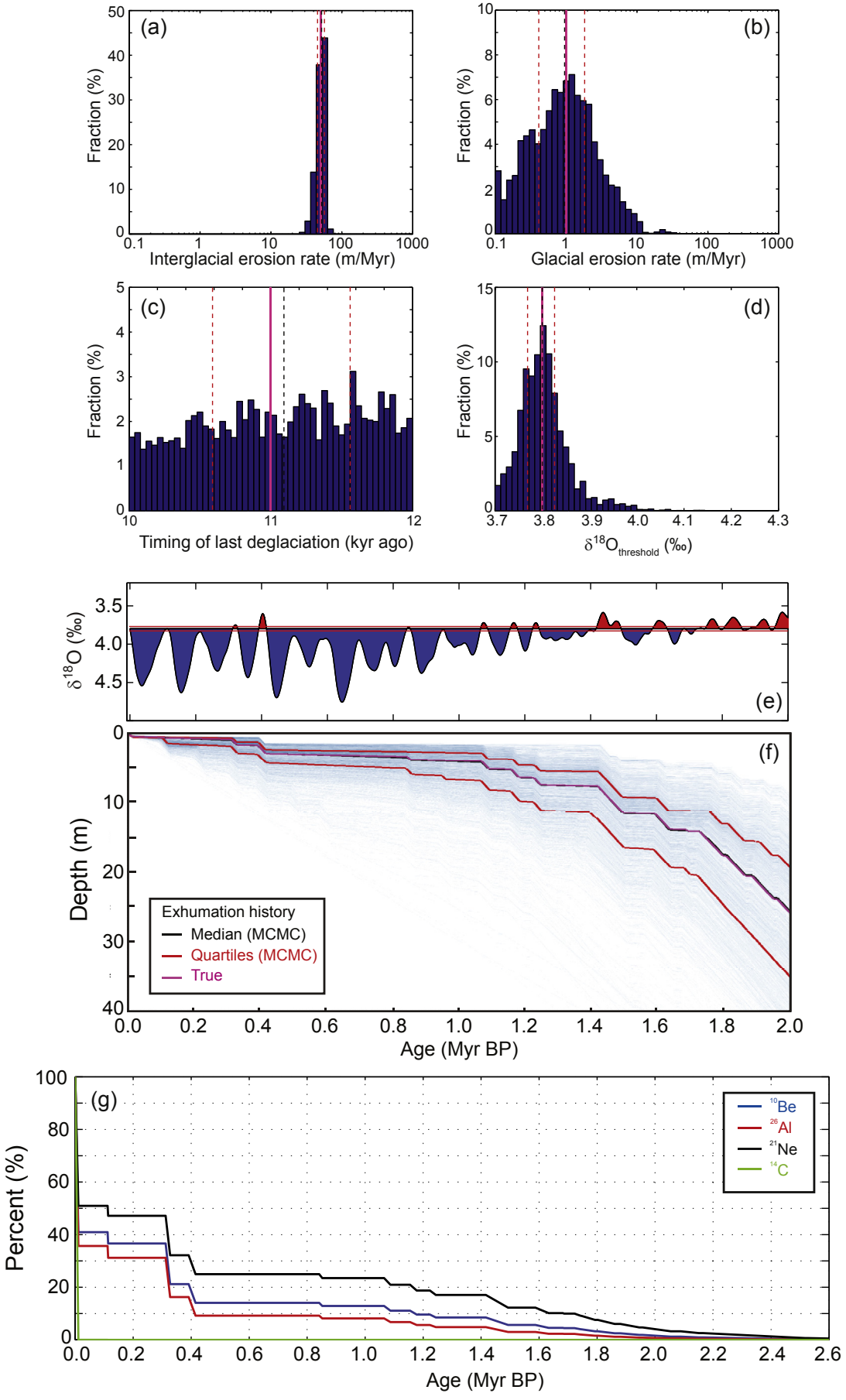
(a)
Fraction (%)
Interglacial erosion rate (m/Myr)
(b)
Glacial erosion rate (m/Myr)
(c)
Timing of last deglaciation (kyr ago)
(d)
δ18Othreshold (‰)
δ18O (‰)
(e)
(f)
Depth (m)
Exhumation history
Median (MCMC)
Quartiles (MCMC)
True
Age (Myr BP)
(g)
Percent (%)
10Be
26Al
21Ne
14C
Age (Myr BP)

American surface production rates for ^{10}Be and ^{26}Al (Balco et al., 2009), whereas the surface production rates of ^{14}C and ^{21}Ne are estimated from the literature (Gosse and Phillips, 2001; Dunai, 2010). For simplicity, a total uncertainty of 5% was assumed for each nuclide. In both scenarios, past glacial-interglacial transitions are estimated by applying a 30-kyr running mean to the global marine δ^{18}O record.

4.1. Synthetic landscape scenario 1

In scenario 1, we simulate a landscape scenario where the glacial erosion rate (ε_{gla} = 1 m/Myr) is considerably lower than the interglacial erosion rate (ε_{int} = 50 m/Myr), thereby leaving a large, inherited cosmogenic inventory from earlier periods of exposure. The glacial-interglacial history is obtained by applying a threshold value of 3.8‰ to the marine benthic oxygen isotope record (Lisiecki and Raymo, 2005), whereas the timing of the last local glacial-interglacial transition (t_{degla} = 11,000 ± 1000 kyr ago) is assumed to be well constrained from studies of glacial erratics. This scenario represents an idealized setting in which the glacial periods were dominated by the presence of cold-based glaciers with little erosive capability, whereas the interglacial periods were characterized by relatively high erosion rates.

For the inverse MCMC approach, the bounds of the model parameters must be specified. For scenario 1, the bounds were as follows: ε_{int} = 0.1–1000 m/Myr; ε_{gla} = 0.1–1000 m/Myr; t_{degla} = 10,000–12,000 years; $\delta^{18}O_{threshold}$ = 3.7–4.3‰. The histograms in Fig. 3 show the range of possible solutions for the four model parameters following 10,000 simulations. The slight skewness of the histograms reflects the non-linearity of the problem. The interglacial erosion rate is very well constrained in this scenario (Fig. 3a), with the median value of 51.7 m/Myr and associated interquartile range (46.1–55.7 m/Myr) reflecting the true interglacial erosion rate (50 m/Myr). The uncertainty estimate is not based on Gaussian distributions, but the fact that 50% of the simulated, best-fitting interglacial erosion rates fall within this range. In general, the interquartile range (middle 50%) provides a robust representation of the uncertainty associated with the estimated model parameters based on the MCMC technique. The low erosion rate associated with glacial periods (Fig. 3b) is not as well defined as the interglacial erosion rate, but the median value of 0.93 m/Myr (0.41–1.85 m/Myr) is very close to the true glacial erosion rate (1 m/Myr). Except for the narrowly defined timing of the last deglaciation (Fig. 3c), the model parameters are generally correctly identified by the MCMC technique, as indicated by the peak distribution of the histograms (Fig. 3). The possible range of exhumation histories is computed from the best-fitting erosion rates and glacial-interglacial transitions ($\delta^{18}O_{threshold}$ and t_{degla}), with the median exhumation history closely tracking the true exhumation history (Fig. 3f). Note that the general change towards low exhumation rates around 1.5–1 Myr ago reflects the emergence of glaciers characterized by an erosion rate that is much lower than the interglacial erosion rate. The median $\delta^{18}O_{threshold}$ value (3.80‰, Fig. 3d) makes it possible to estimate the exposure/burial history throughout the Quaternary (Fig. 3e), which in this synthetic scenario corresponds to the true exposure/burial history. The high interglacial erosion rate (50 m/Myr) and the low degree of exposure during the last 1 Myr imply that a large fraction of all four present-time TCN concentrations were produced during the Holocene, whereas relatively few nuclides derive from the early half of the Quaternary (Fig. 3g).

4.2. Synthetic landscape scenario 2

Synthetic scenario 2 illustrates a setting where the glacial periods are characterized by the inception of warm-based glaciers that erode the landscape more efficiently than the processes operating during the interglacials. However, the glacial erosion is not sufficiently effective to erase the TCNs inherited from previous interglacials. In this scenario, the glacial erosion rate (ε_{gla} = 10 m/Myr) is an order of magnitude higher than the interglacial erosion rate (ε_{int} = 1 m/Myr). The other model parameters are as follows: t_{degla} = 11,000 ± 1000 kyr ago and $\delta^{18}O_{threshold}$ = 4.0‰. The TCN production rates and bounds of the model space, which define the range of possible model parameters investigated with the MCMC technique, remain unchanged compared to scenario 1.

In general, the true model parameters are correctly identified with the MCMC inversion approach in this scenario (Fig. 4). The interglacial and glacial erosion rates are both well constrained (Fig. 4a and b), in particular the interglacial erosion rate, with median values of 1.02 m/Myr (0.95–1.07 m/Myr) and 10.1 m/Myr (6.67–15.1 m/Myr), respectively, which agree with the true interglacial and glacial erosion rates. The $\delta^{18}O_{threshold}$ value is not as well constrained as in scenario 1 (Fig. 4d), but the median value (4.00‰) and interquartile range (3.92–4.11‰) agree well with the true $\delta^{18}O_{threshold}$ value. The full range of possible exhumation histories, encompassing all 10,000 MCMC simulations, displays some scatter (Fig. 4f) due to the uncertainty associated with the estimated $\delta^{18}O_{threshold}$ value, which suggests that a range of exposure/burial histories are possible (Fig. 4e). Nevertheless, the majority of simulated exhumation rates falls within a relatively narrow band, and the median value tracks the true exhumation history closely (magenta line, Fig. 4f). The change in exhumation rate around 1.2 Myr ago reflects the inception of warm-based glaciations characterized by high erosion rates compared to the interglacial periods. The low erosion rate during interglacial periods and the early non-glaciated interval imply that a significant fraction of the present-time ^{10}Be and ^{21}Ne concentrations derive from the early and middle part of the Quaternary, prior to the onset of glaciations 1.2 Myr ago (Fig. 4g). This is particularly true for the radioactively stable ^{21}Ne. The relatively long Eemian interglacial period implies that a significant fraction of the present ^{10}Be and ^{26}Al concentrations were produced during this period, whereas the ^{14}C concentration is completely unaffected by the long Eemian due to its short half-life.

For scenario 2, we also investigate how different sampling and measuring strategies may influence the estimated exhumation history. It is currently common practice to measure concentrations of ^{10}Be and ^{26}Al in boulder and bedrock samples (e.g. Corbett et al., 2013), and we therefore repeated the analyses described above for scenario 2 with the MCMC inversion based solely on the ^{10}Be and

Fig. 4. MCMC inversion results for synthetic landscape scenario 2. The histograms show the distribution of (a) interglacial erosion rates, (b) glacial erosion rate, (c) timing of last deglaciation, and (d) $\delta^{18}O_{threshold}$ levels that provide the best fit to the synthetic TCN concentrations in landscape scenario 2. The fraction indicates the number of simulations included in each bin out of the 10,000 simulations that followed the burn-in phase. (e) The exposure/burial history obtained with the median $\delta^{18}O_{threshold}$ value (c) of the 10,000 simulations in the MCMC inversion analysis. (f) Exhumation histories associated with the best-fitting set of model parameters in the 10,000 simulations (a–d). The depth and time units in (f) were binned and the shading reflects the number of simulations passing through the bins. The black lines in (a–f) denote the median value, whereas the red lines denote the 25% and 75% quartiles. (g) Cumulative contributions during the Quaternary to the present TCN concentrations for synthetic landscape scenario 2 based on the true model parameters (magenta lines in a–d) and true exhumation history (magenta line in f). Note that the short half-life of ^{14}C implies that only the nuclides produced during the Holocene interglacial period contributes to the present ^{14}C concentration. (For interpretation of the references to colour in this figure legend, the reader is referred to the web version of this article.)

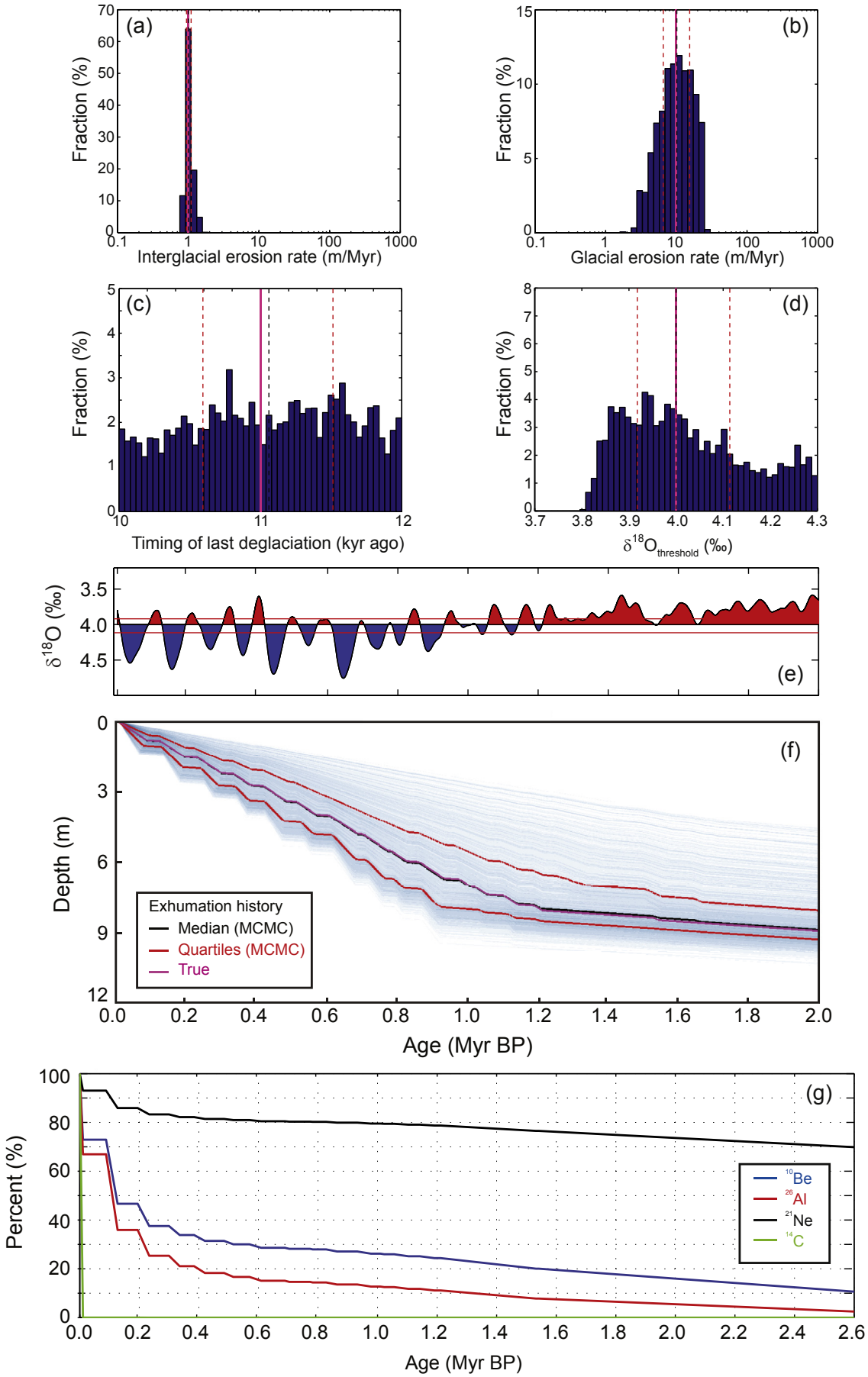
(a)
Fraction (%)
Interglacial erosion rate (m/Myr)
(b)
Fraction (%)
Glacial erosion rate (m/Myr)
(c)
Fraction (%)
Timing of last deglaciation (kyr ago)
(d)
Fraction (%)
δ18Othreshold (‰)
δ18O (‰)
(e)
(f)
Depth (m)
Exhumation history
Median (MCMC)
Quartiles (MCMC)
True
Age (Myr BP)
(g)
Percent (%)
10Be
26Al
21Ne
14C
Age (Myr BP)

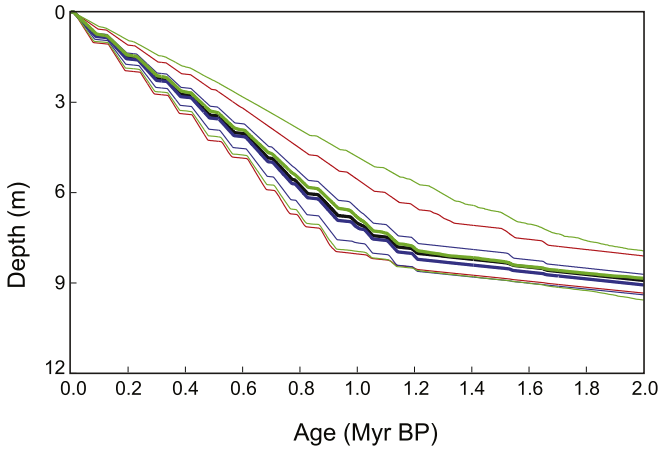

Fig. 5. Exhumation rates for synthetic scenario 2 based on various sampling strategies. The black and red lines represent the median exhumation rate along with the 25% and 75% quartiles based on the concentration of ^{10}Be, ^{26}Al, ^{14}C, and ^{21}Ne at the surface only ($z = 0$ m, similar to Fig. 4). The thick green line represents the median exhumation rate based on the surface ($z = 0$ m) concentration of ^{10}Be and ^{26}Al, whereas the thin green lines represent the associated interquartile range. The thick blue line represents the median exhumation rate based on the concentrations of ^{10}Be, ^{26}Al, ^{14}C, and ^{21}Ne in a vertical profile ($z = 0$, 0.3, 1, 3, 10 m), whereas the thin blue lines represent the associated interquartile range. (For interpretation of the references to colour in this figure legend, the reader is referred to the web version of this article.)

^{26}Al concentrations. In this scenario, the median exhumation history based on ^{10}Be and ^{26}Al is very similar to that based on four nuclides (^{10}Be, ^{26}Al, ^{14}C, and ^{21}Ne) and it also closely resemble the true exhumation history (Fig. 5). However, the model parameters are not quite as well defined as in the analysis based on all four nuclides, and the scatter among the 10,000 individual MCMC simulations is higher, as indicated by the higher interquartile range associated with the estimated exhumation history (Fig. 5). The omission of ^{14}C mainly influences estimates of the interglacial erosion rate, whereas the omission of ^{21}Ne influences the degree to which it is possible to constrain the long-term exposure/burial history. Moreover, with only two data points there is a higher risk that different exhumation histories yield equivalent TCN concentrations, in which case it may be difficult to extract the correct exhumation history. This illustrates the importance of using several random walkers in the inversion approach, as they reveal the robustness of the estimated model parameters. For synthetic landscape scenario 2, we also investigated the effect of measuring all four nuclides in a depth profile ($z = 0$, 0.3, 1, 3, and 10 m). Not surprisingly, the model parameters and the associated estimate of the exhumation history become very well constrained (Fig. 5), but in many scenarios, including the present, it is superfluous to measure several nuclides in a depth profile. However, a depth profile offers the possibility of testing more complex models, involving e.g. varying denudation rates for the different glacial periods.

5. Real landscape scenarios from Upernavik, West Greenland

The two real landscape scenarios included in this section are based on published ^{10}Be and ^{26}Al data from Upernavik, West Greenland (Corbett et al., 2013). Corbett et al. (2013) collected samples along a 100-km northwest–southeast transect perpendicular to the ice margin, using the so-called "dipstick" method where samples are collected at different elevations. Paired bedrock and boulder samples were collected from a range of elevations at each "dipstick", which enable studies of past ice extent, sub-glacial erosion, and exposure history. In general, bedrock samples from high elevations yield the highest single-nuclide ages, and the total minimum-limiting exposure and burial histories indicate a decreasing trend in erosion intensity with increasing elevation. The boulders generally yield lower single-nuclide ages than the bedrock samples, and boulders from low elevations indicate that deglaciation along the northwest–southeast transect occurred rapidly around 11.3 kyr ago (Corbett et al., 2013). In this study, we apply the MCMC model framework to two individual bedrock samples located ~30 km west of the present ice margin in the Upernavik area, including the sample (GU110) yielding the longest total history. For both samples, past glacial-interglacial transitions were estimated by use of a threshold value to a 30-kyr running average of the global marine δ^{18}O.

5.1. High-elevation bedrock sample (GU110) from Upernavik, West Greenland

Bedrock sample GU110 from Upernavik, collected from an altitude of 745 m a.s.l., was included in this analysis, because it yields a long minimum-limiting exposure and burial history (989 kyr). No allochthonous boulders were sampled at this site, but boulders collected from lower elevations in this region suggest that the last deglaciation event occurred around 11.3 kyr ago (Corbett et al., 2013), Following Corbett et al. (2013), we use the northeastern North American production rates (Balco et al., 2009) and the scaling scheme by Lal (1991) and Stone (2000) in CRONUS to obtain the ^{10}Be and ^{26}Al production rates at the sample site. The uncertainties associated with the measured ^{10}Be (5.67×10^5 atoms/g) and ^{26}Al (2.67×10^6 atoms/g) concentrations were 2.6% and 4.0%, respectively.

In the MCMC analysis, the last deglaciation event was constrained to the period 10–12 kyr ago (Fig. 6c), in agreement with ^{10}Be ages from boulders sampled at lower elevations in the area. The MCMC analysis reveals that the interglacial erosion rate must have been less than 7 m/Myr, with the median, and thus most likely, interglacial erosion rate being 1.08 m/Myr (Fig. 6a). An interquartile range of 0.39–2.88 m/Myr indicates that the interglacial erosion rate is not as well constrained as the glacial erosion rate, which has a median value of 1.61 m/Myr and an interquartile range of 0.93–2.28 m/Myr (Fig. 6b). The total median erosion rate, which is not simply the sum of the median glacial and interglacial erosion rates, is 1.57 m/Myr (1.10–2.06 m/Myr), as indicated by median exhumation history (Fig. 6f). This estimate of the most likely exhumation history is robust, as very similar exhumation

Fig. 6. MCMC inversion results based on the concentration of ^{10}Be and ^{26}Al in bedrock sample GU110 collected from a high-elevation surface near Upernavik, West Greenland. The histograms show the distribution of (a) interglacial erosion rates, (b) glacial erosion rate, (c) timing of last deglaciation, and (d) $\delta^{18}O_{threshold}$ levels that provide the best fit to the measured concentrations of ^{10}Be and ^{26}Al. The fraction indicates the number of simulations included in each bin out of the 10,000 simulations that followed the burn-in phase. (e) The exposure/burial history obtained with the median $\delta^{18}O_{threshold}$ value (d) of the 10,000 simulations in the MCMC inversion analysis. (f) Exhumation histories associated with the 10,000 sets of model parameters (a–d). The depth and time units in (f) were binned and the shading reflects the number of simulations passing through the bins. The black lines in (a–f) denote the median value, whereas the red lines denote the 25% and 75% quartiles. (g) Cumulative contributions during the Quaternary to the present concentration of ^{10}Be and ^{26}Al for sample GU110 from Upernavik, West Greenland. The cumulative concentrations of ^{10}Be (blue) and ^{26}Al (red) are based on the median values of the four model parameters associated with 10,000 MCMC simulations (a–d). Note that the low degree of exposure over the last 1 Myr and the low glacial erosion rate imply that a relatively large fraction of the present ^{10}Be and ^{26}Al nuclide inventory were produced more than 1 Myr ago. (For interpretation of the references to colour in this figure legend, the reader is referred to the web version of this article.)

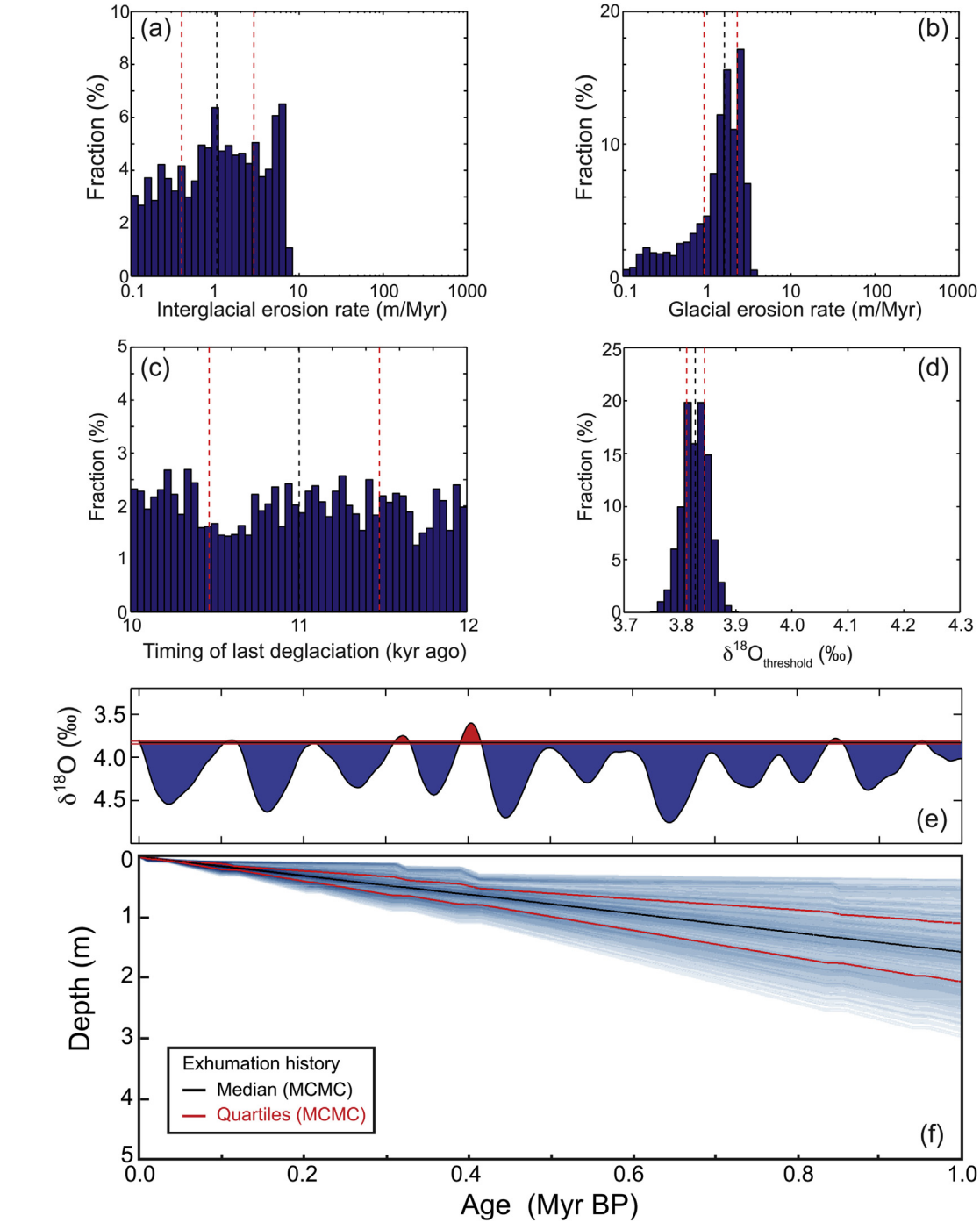
(a)
Fraction (%)
Interglacial erosion rate (m/Myr)
(b)
Fraction (%)
Glacial erosion rate (m/Myr)
(c)
Fraction (%)
Timing of last deglaciation (kyr ago)
(d)
Fraction (%)
δ18Othreshold (‰)
δ18O (‰)
(e)
Depth (m)
Exhumation history
Median (MCMC)
Quartiles (MCMC)
(f)
Age (Myr BP)
(g)
Percent (%)
10Be
26Al
Age (Myr BP)

histories are obtained for different random walkers. Interestingly, the $\delta^{18}O_{threshold}$ value is also very well constrained, suggesting that the exposure history is defined by a threshold value of 3.83‰ (3.81–3.84‰, Fig. 6d). Such a $\delta^{18}O_{threshold}$ value implies that the total amount of exposure within the last million years was limited to the range 80–110 kyr, of which ~26 kyr of exposure occurred during MIS (marine isotope stage) 11 around 400 kyr ago (Fig. 6e). The low degree of exposure over the past 1 Myr implies that considerable fractions of the present ^{10}Be and ^{26}Al concentrations are inherited from periods of exposure prior to the last 1 Myr (Fig. 6g). The limited amount of exposure is highly consistent with the minimum-limiting exposure duration (88 kyr) and burial duration (901 kyr) based on the two-isotope burial–exposure diagram (Corbett et al., 2013).

5.2. Intermediate-elevation bedrock sample (GU111) from Upernavik, West Greenland

In this analysis of real TCN data, we also include bedrock sample GU111 from Upernavik, West Greenland. This sample, which was collected from the same "dipstick" as sample GU110, albeit from a lower elevation (325 m a.s.l.), yields a minimum-limiting total history of 526 kyr (Corbett et al., 2013). As for sample GU110, we use the northeastern North American production rates (Balco et al., 2009) and the CRONUS-Earth on-line calculator to get the ^{10}Be and ^{26}Al production rates, and the timing of the last deglaciation is constrained to the period 10–12 kyr ago (Fig. 7c). The MCMC inversion analysis of the measured ^{10}Be (4.26×10^5 atoms/g) and ^{26}Al (2.37×10^6 atoms/g) concentrations yields reasonably well defined erosion rates, with a median interglacial erosion rate of 1.80 m/Myr (1.02–3.04 m/Myr, Fig. 7a) and a median glacial erosion rate of 4.16 m/Myr (2.64–6.07 m/Myr, Fig. 7b). A median δ^{18}O-threshold value of 4.00‰ (3.94–4.07‰, Fig. 7d) suggests that site GU111 was more exposed than site GU110, with several long-lasting (~15–20 kyr) non-glaciated periods over the last Myr (Fig. 7e). This is in agreement with existing minimum-limiting exposure and burial ages, suggesting that sample GU111 was exposed for a larger fraction than its total history compared to sample GU110 (Corbett et al., 2013). The exhumation history for sample GU111 shows a total median erosion rate of 3.47 m/Myr (2.77–4.06, Fig. 7f), i.e. more than twice the total median erosion rate obtained for sample GU110 (1.57 m/Myr). The relatively high exhumation rate, along with the more frequent and longer interglacial periods, imply that larger fractions of the present ^{10}Be and ^{21}Al concentrations were acquired during the most recent interglacials for sample GU111 in comparison to sample GU110 (Fig. 7g).

Overall, the MCMC inversion analyses indicate that the total denudation rate at the high-elevation surfaces was less than half the denudation rate at intermediate elevations. These quantitative results agree well with the conclusions of Corbett et al. (2013), suggesting that efficient glacial erosion occurred at low elevations with a decreasing trend in glacial erosivity towards higher elevations, most likely due to the presence of non-erosive, cold-based ice at high-elevation surfaces over numerous glacial cycles.

6. Discussion

The framework presented here provides a highly flexible multi-nuclide approach to delineate likely landscape histories and past erosion rates in terrains previously covered by ice masses. The approach is designed to be applicable to a wide range of specific geological settings and problems. As such, the user may specify the production rates due to spallation and muons at the study site, the attenuation lengths, the rock density, the number of cosmogenic nuclides used in the study (e.g. ^{10}Be, ^{26}Al or ^{10}Be, ^{26}Al, ^{14}C, ^{21}Ne), the measured concentrations and associated uncertainties as well as the sample depths (e.g. $z = 0$ m or $z = 0, 0.5, 1$ m). It is also possible to specify various kinds of information regarding past glacial-interglacial transition times. Likewise, if any of the model parameters are well constrained from other studies, a narrow bound should be specified for these parameters for the MCMC inversion. Nevertheless, the general approach contains some rather simplistic assumptions concerning the choice of model parameters related to past glacial-interglacial transition times and past erosion rates that are subject to debate.

6.1. Estimating the glacial-interglacial exposure history

In many cases, it is possible to estimate the timing of the last deglacial transition, e.g. via ^{10}Be dating of erratic boulders or terminal moraines, whereas no information regarding earlier transitions is available. For such scenarios, this study provides an approach to constrain these unknowns based on a two-stage glacial-interglacial model calibrated to changes in global climate. This approach is appealing, because the regional extent of glaciations is likely to correlate with changes in global climate. This may not be true locally, however, as the occurrence of past glaciations depends on local climate and altitude. It is also unknown if the assumption regarding 100% shielding during glacial periods is reasonable, as it would require >10 m of ice to render the production due to spallation negligible (>50 m for muons). The cumulative effects of snow shielding during interglacials are also uncertain and potentially important (Schildgen et al., 2005; Dunai et al., 2014; Delunel et al., 2014). However, it is possible to correct for such effects by introducing a correction factor in the model, provided the effect is well constrained.

Another aspect concerns the temporal resolution at which glaciations occur, e.g., did MIS 5 comprise a warm, ice-free interval, including the Eemian (MIS 5e), and a series of relatively brief glaciations? A recent study by Mangerud et al. (2011) shows that in Scandinavia the stadials following the Eemian were marked by glacial advances lasting 5–10 kyr. These changes are very consistent with the glacial-interglacial history obtained by applying a 5-kyr running mean to the marine δ^{18}O record, whereas the 30-kyr running mean used in this study produces a somewhat simpler exposure history. For most scenarios, however, the resolution of the marine δ^{18}O record has a limited effect on the concentration of cosmogenic nuclides. The application of different $\delta^{18}O_{threshold}$ levels generally result in considerably larger differences in TCN concentrations because changes in the $\delta^{18}O_{threshold}$ level significantly influence the ratio between glacial and interglacial times. It remains

Fig. 7. MCMC inversion results based on the concentration of ^{10}Be and ^{26}Al in bedrock sample GU111 collected from intermediate elevations near Upernavik, West Greenland. The histograms show the distribution of (a) interglacial erosion rates, (b) glacial erosion rate, (c) timing of last deglaciation, and (d) $\delta^{18}O_{threshold}$ levels that provide the best fit to the measured concentrations of ^{10}Be and ^{26}Al. The fraction indicates the number of simulations included in each bin out of the 10,000 simulations that followed the burn-in phase. (e) The exposure/burial history obtained with the median $\delta^{18}O_{threshold}$ value (d) of the 10,000 simulations in the MCMC inversion analysis. (f) Exhumation histories associated with the 10,000 sets of model parameters (a–d). The depth and time units in (f) were binned and the shading reflects the number of simulations passing through the bins. The black lines in (a–f) denote the median value, whereas the red lines denote the 25% and 75% quartiles. (g) Cumulative contributions during the Quaternary to the present concentration of ^{10}Be and ^{26}Al for sample GU111 from Upernavik, West Greenland. The cumulative concentrations of ^{10}Be (blue) and ^{26}Al (red) are based on the median values of the four model parameters associated with 10,000 MCMC simulations (a–d). (For interpretation of the references to colour in this figure legend, the reader is referred to the web version of this article.)

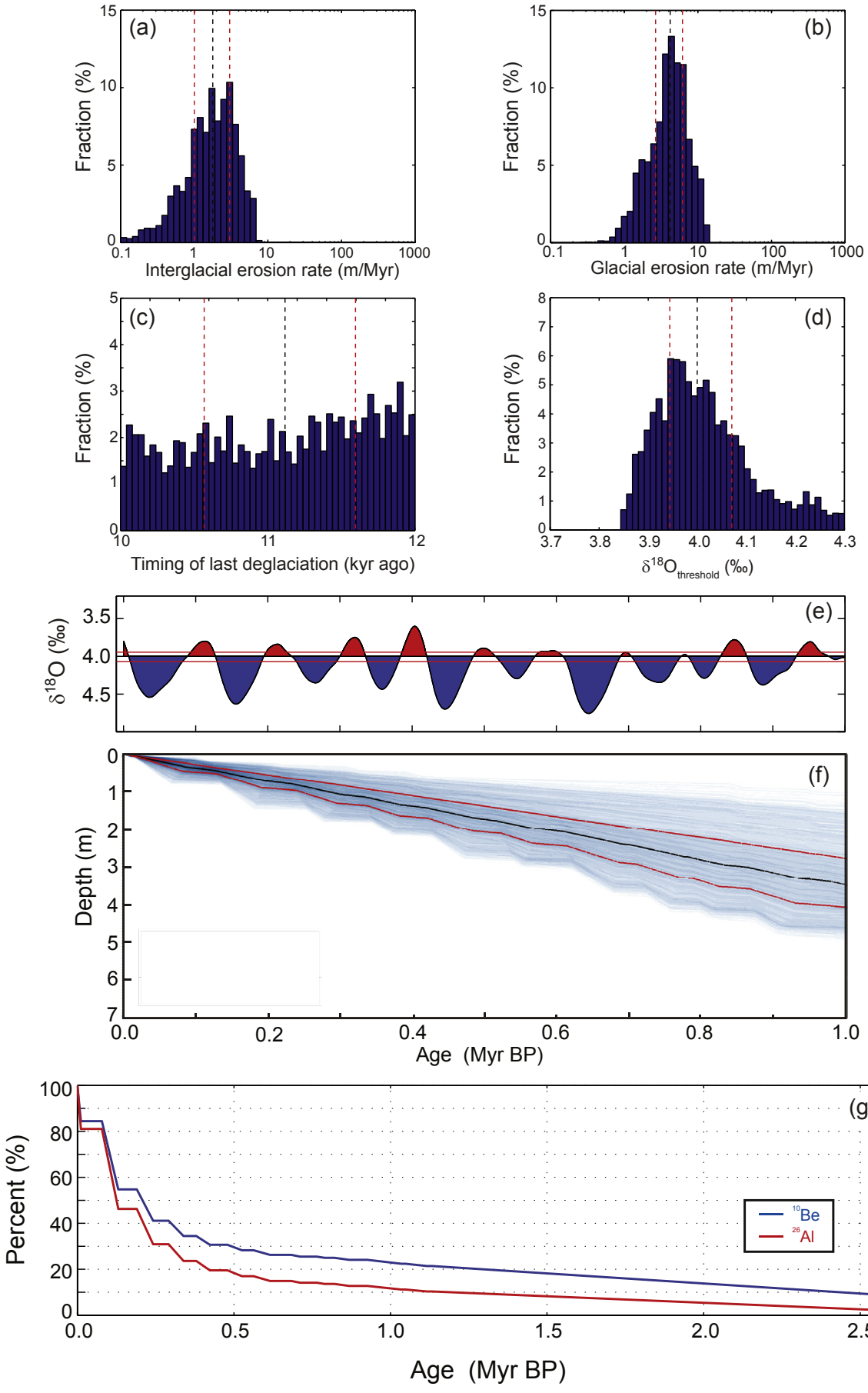
(a)
Fraction (%)
Interglacial erosion rate (m/Myr)
(b)
Glacial erosion rate (m/Myr)
(c)
Timing of last deglaciation (kyr ago)
(d)
δ18Othreshold (‰)
(e)
δ18O (‰)
(f)
Depth (m)
Age (Myr BP)
(g)
Percent (%)
10Be
26Al
Age (Myr BP)

an open question, however, whether it is meaningful to define the glacial history throughout the Quaternary based on a constant $\delta^{18}O_{threshold}$ level, as the long-term cooling trend during the Quaternary potentially influenced this threshold level. Yet, for the majority of geological settings this is unlikely to represent a large problem because the present TCN concentrations are dominated by the more recent glacial-interglacial cycles, where the long-term trend in the $\delta^{18}O$ record is relatively small. In contrast, for geological settings characterized by very low exhumation rates and a low degree of exposure over the past 1 Myr, the effect may be significant. For such settings, it may be possible to study these effects due to the significant contribution to the present TCN contributions from exposures during the early-middle part of the Quaternary, in particular if the radioactively stable ^{21}Ne is included.

6.2. The concept of locally constant glacial and interglacial erosion rate

The assumption of one uniform erosion rate across all interglacial periods and another uniform erosion rate across all glacial periods is obviously simplistic, but it is difficult to assess the validity of this assumption. It is clear that multiple climate-dependent erosion processes, which varied greatly over short timespans, must have accompanied the growth and decay of ice masses throughout the Quaternary. For instance, each deglaciation yields prodigious volumes of meltwater and debris resulting in major episodes of erosion and deposition along proglacial river valleys (Ballantyne, 2002); and secondly, interglacials bring periglacial activity, which fluctuates in intensity according to mean annual temperatures that vary considerably over time (Hales and Roering, 2007). Nevertheless, it is likely that the same short-term evolution was more or less repeated over multiple glacial cycles and that average erosion rates of, for example, different glacial periods were largely similar. Furthermore, the average erosion rates over full glacial and interglacial periods, respectively, were likely dominated by fundamentally different processes and our two-stage model is designed to resolve the differences between these two regimes. Accounting for varying denudation rates during glacial periods would render the problem intractable unless several nuclides are measured from a depth profile, because the inclusion of additional free parameters linked to erosion rate would also imply additional free parameters linked to the associated timespans. We thus believe the current model framework provides a reasonable balance between observations and number of free model parameters. We emphasize that the concept of a glacial and an interglacial erosion rate implies that the estimated rates represent gross averages across glacials and interglacials, respectively, and thus should be interpreted within this framework.

6.3. Other applications of the model framework

The potential application of the model framework presented here is not limited to constraining past erosion rates in previously glaciated terrains. This approach can be applied to a variety of landscape settings characterized by a complex exposure history and erosion rates that vary in time. For instance, the model may be used to investigate temporal changes in erosion rate in non-glacial, fluvial landscapes, and help constrain whether erosion rates increased in sync with the global cooling trend, as suggested by e.g. Herman et al. (2013). It may also be used in regions characterized by high glacial and interglacial denudation rates, such as the Southern Alps and the Himalayas, to constrain the timing of the last deglaciation event as well as the denudation rate during the ensuing non-glaciated period.

The model framework may also be combined with numerical landscape simulations (e.g Egholm et al., 2012; Egholm et al., 2013) that produce virtual, process-dependent, landscape histories, which otherwise may be difficult to link-up with real, specific landscapes. The forward model presented in this study makes it possible to calculate the virtual TCN concentrations for any simulated landscape history, which then may be compared to measured concentrations based on field studies. This application does not involve any two-stage model assumptions regarding past glacial-interglacial transitions and associated erosion rates, because the exhumation history and ice cover can be tracked through time at any point in the model simulation. In this way, the model framework presented here offers a potentially useful tool to explore and identify dominant landscape processes by testing and calibrating physics-based models. It may also be used to design sampling strategies based on expected patterns in cosmogenic nuclide concentrations linked to local variations in exposure history and erosion rates.

7. Future perspectives

We have developed a model framework that is designed to constrain the most likely landscape history and past erosion rates, based on multiple cosmogenic nuclides, in regions characterized by a complex exposure history. The current approach focuses mainly on terrains that experienced the waxing and waning of thick glacial ice masses during numerous glacial-interglacial cycles, but the method is highly flexible and can be applied to a wide range of geological settings. Currently, the model framework includes the following cosmogenic nuclides ^{10}Be, ^{26}Al, ^{14}C, and ^{21}Ne, but it is relatively straightforward to incorporate other nuclides, such as ^{36}Cl and ^{3}He, in the future so as to further constrain the inverse problem. Similarly, it is also possible to include isostatic rebound effects, provided the magnitude of this effect can be estimated from other sources. This may be particularly relevant for efforts to integrate the computation of landscape-wide TCN concentrations with physics-based landscape simulations where the isostatic rebound effect is known.

Acknowledgments

Mads Faurschou Knudsen is grateful for financial support from the Villum Foundation (VKR023114) and Geocenter Denmark (Geocenterbevilling 1-2014). Egholm acknowledges support from the Aarhus University Research Foundation, while John Jansen was supported by a BRAIN-Marie Curie Fellowship. We thank two anonymous reviewers for highly constructive comments.

References

Anderson, R.S., Repka, J.L., Dick, G.S., 1996. Explicit treatment of inheritance in dating depositional surfaces using in situ ^{10}Be and ^{26}Al. Geology 24, 47–51.

Balco, G., Stone, J.O., Lifton, N.A., Dunai, T., 2008. A complete and easily accessible means of calculating surface exposure ages or erosion rates from ^{10}Be and ^{26}Al measurements. Quat. Geochronol. 3, 174–195.

Balco, G., Shuster, D.L., 2009. ^{26}Al–^{10}Be–^{21}Ne burial dating. Earth Planet. Sci. Lett. 286, 570–575.

Balco, G., Briner, J., Finkel, R.C., Rayburn, J.A., Ridge, J.C., Schaefer, J.M., 2009. Regional beryllium-10 production rate calibration for northeastern North America. Quat. Geochronol. 4, 93–107.

Ballantyne, C.K., 2002. A general model of paraglacial landscape response. Holocene 12 (3), 371–376.

Bierman, P.R., Marsella, K.A., Patterson, C., Davis, P.T., Caffee, M., 1999. Mid-Pleistocene cosmogenic minimum-age limits for pre-Wisconsinan glacial surfaces in southwestern Minnesota and southern Baffin Island; a multiple nuclide approach. Geomorphology 27, 25–39.

Braucher, R., Del Castillo, P., Siame, L., Hidy, A.J., Bourlès, D.L., 2009. Determination of both exposure time and denudation rate from an in situ-produced ^{10}Be depth profile: a mathematical proof of uniqueness. Model sensitivity and applications to natural cases. Quat. Geochronol. 4 (1), 56–67.

Braucher, R., Bourlès, D., Merchel, S., Vidal Romani, J., Fernadez-Mosquera, D.,

Marty, K., Léanni, L., Chauvet, F., Arnold, M., Aumaître, G., Keddadouche, K., 2013. Determination of muon attenuation lengths in depth profiles from in situ produced cosmogenic nuclides. Nucl. Instrm. Methods Phys. Res. B 294, 484–490.

Braucher, R., Merchel, S., Borgomano, J., Bourlès, D.L., 2011. Production of cosmogenic radionuclides at great depth: a multi element approach. Earth Planet. Sci. Lett. 309, 1–9.

Corbett, L.B., Bierman, P.R., Graly, J.A., Neumann, T.A., Rood, D.H., 2013. Constraining landscape history and glacial erosivity using paired cosmogenic nuclides in Upernavik, northwest Greenland. Geol. Soc. Am. Bull. http://dx.doi.org/10.1130/B30813.1.

Delunel, R., Bourlès, D.L., van der Beek, P.A., Schlunegger, F., Leya, I., Masarik, J., Paquet, E., 2014. Snow shielding factors for cosmogenic nuclide dating inferred from long-term neutron detector monitoring. Quat. Geochronol. 24, 16–26.

Dunai, T.J., 2001. Influence of secular variation of the magnetic field on production rates of in situ produced cosmogenic nuclides. Earth Planet. Sci. Lett. 193, 197–212.

Dunai, T.J., 2010. Cosmogenic Nuclides: Principles, Concepts and Applications in the Earth Surface Sciences. Cambridge University Press, Cambridge, UK.

Dunai, T.J., Binnie, S.A., Hein, A.S., Paling, S.M., 2014. The effects of a hydrogen-rich ground cover on cosmogenic thermal neutrons: Implications for exposure dating. Quat. Geochronol. 22, 183–191.

Egholm, D.L., Pedersen, V.K., Knudsen, M.F., Larsen, N.K., 2012. Coupling the flow of ice, water, and sediment in a glacial landscape evolution model. Geomorphology 141–142, 47–66.

Egholm, D.L., Knudsen, M.F., Sandiford, M., 2013. Lifespan of mountain ranges scaled by feedbacks between landsliding and erosion by rivers. Nature 498, 475–478.

Fabel, D., Stroeven, A.P., Harbor, J., Kleman, J., Elmore, D., Fink, D., 2002. Earth Planet. Sci. Lett. 201, 397–406.

Gelman, A., Roberts, G.O., Gilks, W.R., 1996. Efficient metropolis jumping rules. In: Bayesian Statistics, vol. 5. Clarendon, Oxford, UK, pp. 599–608.

Gosse, J.C., Phillips, F.M., 2001. Terrestrial in situ cosmogenic nuclides: theory and application. Quat. Sci. Rev. 20, 1475–1560.

Granger, D.E., Smith, A.L., 2000. Dating buried sediments using radioactive decay and muogenic production of ^{26}Al and ^{10}Be. Nucl. Instrum. Methods Phys. Res. Sect. B 172, 822–826.

Granger, D.E., 2006. A review of burial dating methods using ^{26}Al and ^{10}Be. In: Siame, L., Bourlès, D.L., Brown, E.T. (Eds.), In Situ-produced Cosmogenic Nuclides and Quantification of Geological Processes, pp. 1–16. Geological Society of America Special Paper 415.

Haeuselmann, P., Granger, D.E., Jeanin, P.-Y., Lauritsen, S.-E., 2007. Abrupt glacial valley incision at 0.8 Ma dated from cave deposits in Switzerland. Geology 35, 143–146.

Hales, T.C., Roering, J.J., 2007. Climatic controls on frost cracking and implications for the evolution of bedrock landscapes. J. Geophys. Res. Earth Surf. 112, F2 (2003–2012).

Hancock, G.S., Anderson, R.S., 2002. Numerical modeling of fluvial strath-terrace formation in response to oscillating climate. Geol. Soc. Am. Bull. 114 (9), 1131–1142. http://dx.doi.org/10.1130/0016-7606(2002)114.

Hastings, W.K., 1970. Monte carlo sampling methods using markov Chains and their applications. Biometrika 57 (1), 97–109.

Heisinger, B., Lal, D., Jull, A.J.T., Kubik, P., Ivy-Ochs, S., Neumaier, S., Knie, K., Lazarev, V., Nolte, E., 2002a. Pro- duction of selected cosmogenic radionuclides by muons: 1. fast muons. Earth Planet. Sci. Lett. 200, 345–355.

Heisinger, B., Lal, D., Jull, A.J.T., Kubik, P., Ivy-Ochs, S., Knie, K., Nolte, E., 2002b. Production of selected cos- mogenic radionuclides by muons: 2. capture of negative muons. Earth Planet. Sci. Lett. 200, 357–369.

Herman, F., Seward, D., Valla, P.G., Carter, A., Kohn, B., Willett, S.D., Ehlers, T.A., 2013. Worldwide acceleration of mountain erosion under a cooling climate. Nature 504, 423–426.

Hidy, A.J., Gosse, J.C., Pederson, J.L., Mattern, J.P., Finkel, R.C., 2010. A geologically constrained Monte Carlo approach to modeling exposure ages from profiles of cosmogenic nuclides: an example from Lees Ferry, Arizona. Geochem. Geophys. Geosystems 11, 1–18.

Hidy, A.J., Gosse, J.C., Blum, M.D., Gibling, M.R., 2014. Glacial-interglacial variation in denudation rates from interior texas, USA, established with cosmogenic nuclides. Earth Planet. Sci. Lett. 390, 209–221.

Kleman, J., Stroeven, A.P., 1997. Periglacial surface remnants and quaternary glacial regimes in northwestern Sweden. Geomorphology 19 (1), 35–54.

Kleman, J., Lundqvist, J., Stroeven, A.P., 2008. Patterns of quaternary ice sheet erosion and deposition in Fennoscandia. Geomorphology 97, 73–90.

Lal, D., 1991. Cosmic ray labeling of erosion surfaces: in situ nuclide production rates and erosion models. Earth Planet. Sci. Lett. 104, 424–439.

Lal, D., Peters, B., 1967. Cosmic ray produced radioactivity on the earth. In: Sitte, K. (Ed.), Handbuch der Physik. Springer, Berlin, pp. 551–612.

Levy, L.B., Kelly, M.A., Lowell, T.V., Hall, B.L., Hempel, L.A., Honsaker, W.M., Lusas, A.R., Howley, J.A., Axford, Y.L., 2014. Holocene fluctuations of Bregne ice cap, Scoresby Sund, east Greenland: a proxy for climate along the Greenland ice sheet margin. Quat. Sci. Rev. 92, 357–368.

Lifton, N., Bieber, J., Clem, J., Duldig, M., Evenson, P., Humble, J., Pyle, R., 2005. Addressing solar modulation and long-term un- certainties in scaling secondary cosmic rays for in situ cosmogenic nuclide applications. Earth Planet. Sci. Lett. 239, 140–161.

Lisiecki, L.E., Raymo, M.E., 2005. A Pliocene-Pleistocene stack of 57 globally distributed benthic δ^{18}O records. Paleoceanography 20 (1), PA1003, 1–17.

Mangerud, J., Gyllencreutz, R., Lohne, Ø., Svendsen, J.I., 2011. Glacial history of Norway. Dev. Quat. Sci. 15, 279–298.

Metropolis, N., Rosenbluth, A.W., Rosenbluth, M.N., Teller, A.H., Teller, E., 1953. Equations of state calculations by fast computing machines. J. Chem. Phys. 21 (6), 1087–1092.

Niedermann, S., Graf, T., Kim, J.S., Kohl, C.P., Marti, K., Nishiizumi, K., 1994. Cosmic-ray produced 21Ne in terrestrial quartz: the neon inventory of Sierra Nevada quartz separates. Earth Planet. Sci. Lett. 125, 341–355.

Niedermann, S., 2002. Cosmic-ray-produced noble gases in terrestrial rocks: dating tools for surface processes. Rev. Mineral. Geochem 47, 731–784.

Schaller, M., von Blanckenburg, F., Veldkamp, A., Tebbens, L.A., Hovius, N., Kubik, P.W., 2002. A 30000 yr record of erosion rates from cosmogenic ^{10}Be in Middle European river terraces. Earth Planet. Sci. Lett. 204, 307–320.

Schildgen, T.F., Purves, R.S., Phillips, W.M., 2005. Simulation of snow shielding corrections for cosmogenic nuclide surface exposure studies. Geomorphology 64, 67–85.

Shuster, D.L., Ehlers, T.A., Rusmoren, M.E., Farley, K.A., 2005. Rapid glacial erosion at 1.8 Ma revealed by ^{4}He/^{3}He thermochronometry. Science 310, 1668–1670.

Stone, J.O., 2000. Air pressure and cosmogenic isotope production. J. Geophys. Res. 105 (B10), 23753–23759.

Thomson, S.N., Brandon, M.T., Tomkin, J.H., Reiners, P.W., Vásquez, C., Wilson, N.J., 2010. Glaciations as a destructive and constructive control on mountain building. Nature 467, 313–317.

Tucker, G.E., McCoy, S.W., Whittaker, A.C., Roberts, G.P., Lancaster, S.T., Phillips, R., 2011. Geomorphic significance of postglacial bedrock scarps on normal-fault footwalls. J. Geophys. Earth Surf. 116 (F1) http://dx.doi.org/10.1029/2010JF001861.

von Blanckenburg, F., 2005. The control mechanisms of erosion and weathering at basin scale from cosmogenic nuclides in river sediment. Earth Planet. Sci. Lett. 237, 462–479.

Zhang, P., Molnar, P., Downs, W.R., 2001. Increased sedimentation rates and grain sizes 2-4 Myr ago due to the influence of climate change on erosion rates. Nature 410, 891–897.